Aerosols and Temperature Rise in the Northwestern Himalaya, India

Jagdish Chandra Kuniyal

Abstract Aerosols, the important constituents of our atmosphere, indicate a colloidal system of particulate, gaseous and volatile organic compounds. Aerosols play a significant role in affecting adversely the radiative balance of the Earth as well as the air temperature. Moreover, these not only influence the visibility and overall air quality, but also adversely affect health of living organisms in an ecosystem. In this context, the present attempt at Mohal (1,154 m, 77.12°E, 31.91°N) in the Kullu valley of Himachal Pradesh in the northwestern Himalayan region explains the ever increasing columnar aerosols, their relationship with black carbon (BC) aerosols, impact of local meteorological conditions, long range transport sources and their collective impact on radiative forcing and resultant temperature rise. The aerosol optical depth (AOD) having been under observation for the last half a decade (2006–2010) shows higher values at shorter wavelengths and lower at longer wavelengths. At a representative wavelength of 500 nm, AOD is found to be increasing at the rate of 1.9 % per annum from 2006 to 2010. Overall, AOD values in all the wavelengths (380–1,025 nm) were found between 0.238–0.242, reflecting an increasing trend at the rate of 0.84 % per annum. The monthly mean concentration of BC aerosols is noticed maximum with 6,617 ng m^{-3} in January, 2010. The pollution loads in terms of AOD values translate into a temperature rise by ~0.54 K day^{-1}. The local as well as transported aerosols together contribute to the existing aerosols in the present study region. The local sources possibly belong to anthropogenic aerosols including vehicular emissions, biomass burning (like fuel wood for cooking), forest fires, open waste burning, etc. While the transported aerosols most probably include fine mineral dust from the desert regions and the sulphate aerosol from the oceanic regions with the movement of air masses prior to the western disturbances and monsoonal winds in the region.

J.C. Kuniyal (✉)
G. B. Pant Institute of Himalayan Environment and Development,
Himachal Unit, Mohal-Kullu, Himachal Pradesh, India
e-mail: jckuniyal@gmail.com

1 Introduction

The study of aerosols, in modern science, is not only interesting but is also growing popular day by day. Aerosols are the colloidal system of particulate, gaseous and liquid pollutants which remain in suspension in the Earth's atmosphere (Iqbal 1983). The most important optical properties of the aerosols is the aerosol optical depth (AOD) which is directly proportional to the magnitude of the attenuation of direct solar radiation by scattering and absorption process (Charlson et al. 1992). If the aerosols remain with higher concentrations in the atmosphere, these may have impacts either on human health or plant life (Liu et al. 1991) or climate impacts causing radiative forcing, temperature rise and ultimately climate change. Fine size particles are primarily generated through anthropogenic activities. The process of gas to particle conversion is responsible for a variety of the other forms of pollution like haze, mist and fog. These pollutions are responsible for respiratory problems in human beings which may become a cause of carcinogen.

The Himalayan region is considered as a white box in terms of availability of data on aerosols which may have long-term effects in temperature rise. It is, therefore, very important to conduct study on aerosols in the sub-mountain region of the Indian Himalaya similar to the Indo-Gangetic Plain (Singh et al. 2008), northwestern Himalaya (Kuniyal et al. 2007, 2009), and other parts of the western, eastern, and coastal regions of the country (Beegum et al. 2008). Himalaya being considered as the third pole after Antarctica and Arctic; studies beyond Indian Himalayan Region (IHR), around the Tibetan plateau (Liu et al. 2008) and other parts of the Hindu-kush Himalayan region are rare. The solar energy reaching at top of the atmosphere (TOA) arrives at the Earth's surface with attenuation mainly due to aerosols and other atmospheric factors. Some amount of the radiant energy is reflected back into the space, while some is absorbed by the aerosols within the atmosphere. However, the reflective and absorptive solar energy depends much on their nature and quality of aerosols in the atmosphere. Sulphate, the oceanic aerosol, has reflective quality (Moorthy et al. 1998; Satheesh et al. 2001), while black carbon, the carbonaceous aerosol produced mostly from the local biomass burning sources, has a heat absorbing quality. So depending on the nature of aerosols, cooling effect mostly near the surface as well as at top of the atmosphere and warming effect in the atmosphere together result in the radiative imbalance. This phenomenon from local to regional level later has implications in existing climate of a particular geographic entity. The process of scattering and absorption of solar irradiance or incoming solar radiation alter the radiation budget of the Earth's atmosphere (Fu and Liou 1992, 1993) which in due course results for changes in climate (IPCC 2007).

Keeping in view of these issues pertaining to aerosols, temperature rise and climate change, the present study is carried out with the objectives to: (i) obtain

aerosol optical depth (AOD) in ultra-violet, visible and near infrared wavelengths (380–1,025 nm), (ii) estimate the concentration of black carbon aerosols, (iii) identify the possible local and external pollution sources estimating vehicular influx, etc. and HYSPLIT model of back trajectory analysis respectively, and (iv) monitor aerosol impact on temperature rise and hence on climate change in the region.

2 Experimental Site and Methodology

The observations for AOD, black carbon (BC) and meteorological parameters were carried out at Mohal (1,154 amsl, 77.12°E, 31.91°N), located at 5 km south to Kullu town, in the northwestern Indian Himalayan region. The experimental site is located within the campus of Himachal Unit of G. B. Pant Institute of Himalayan Environment and Development, at Mohal-Kullu, Himachal Pradesh. The distance of the sampling site from the National Highway (NH)-21 is about 288 m, while direction of the experimental site from the NH-21 is in the north–west.

The measurements of AOD, BC and meteorological parameters were carried out using the Multi-wavelength Radiometer (MWR), Aethalometer, and Automatic Weather Station (AWS), respectively. The MWR instrument works on the principle of filter wheel radiometer as described by Shaw et al. (1973). The MWR, developed at Space Physics Laboratory, Vikram Sarabhai Space Centre, Thiruvanthapuram, has ten wavelength bands, centered at 380, 400, 450, 500, 600, 650, 750, 850, 935 and 1,025 nm (Moorthy et al. 1999; Bhuyan et al. 2005; Gogoi et al. 2008, 2009), whereas the field of view of the MWR instrument is 2° (Moorthy et al. 1999). From each set of MWR measurements, the columnar optical depths (τ_λ) were estimated using the Langley technique by making a linear regression fit to Bouger-Lambert-Beer Law (Moorthy et al. 1999) as follows,

$$\ln E_\lambda = \ln E_{o\lambda} + 2 \ln (d_o/d) - m\tau_\lambda \tag{1}$$

where E_λ represents the ground reaching solar radiation, $E_{o\lambda}$ indicates the solar radiation incident at the top of the atmosphere, d_o and d are the mean and instantaneous values of the Sun-Earth distance, m indicates the relative air-mass as a function of Solar Zenith Angle $\leq 70°$.

The τ_λ obtained from Eq. 1 explains the total columnar optical depth as an outcome of different atmospheric extinction processes, i.e., scattering due to air molecules ($\tau_{r\lambda}$), aerosols ($\tau_{p\lambda}$), gaseous (i.e. ozone and nitrogen dioxide) and water vapour absorption ($\tau_{\alpha\lambda}$) (Moorthy et al. 1991, 1996),

$$\tau_\lambda = \tau_{r\lambda} + \tau_{\alpha\lambda} + \tau_{p\lambda} \tag{2}$$

Thereafter, $\tau_{p\lambda}$ is estimated for each observation day using Eq. (2) (Moorthy et al. 1996) as under,

$$\tau_{p\lambda} = \tau_\lambda - (\tau_{r\lambda} + \tau_{\alpha\lambda}) \tag{3}$$

The spectral dependence of AOD is used to compute Ångström exponent (α) and turbidity coefficient (β) in the wavelength interval 0.38–1.025 μm by making a linear regression fit to Ångström Power Law (Ångström 1961),

$$\tau_{p\lambda} = \beta\,\lambda^{-\alpha} \tag{4}$$

The continuous and near-real-time measurements of the mass concentration of black carbon aerosols were carried out using Aethalometer (Model AE-31-ER, Magee Scientific, USA). Aethalometer works based on the attenuation of a beam of light transmitted through a quartz fiber filter tape which continuously collects aerosol sample from ambient air (Raju et al. 2011). The instrument is operated at an average time of 5 min, round the clock with a flow rate of 2.9 L m^{-1}. The BC mass concentration is estimated by measuring the change in the transmittance of a quartz filter tape (Hansen et al. 1984). The optical attenuation (ATN) is explained as follows (Hansen 2005),

$$ATN = 100 \times \ln(I_o/I) \tag{5}$$

where I_o = intensity of the light transmitted through the original filter/blank portion, I = intensity of the light transmitted through the portion of the filter on which BC is collected, 100 corresponds to an aerosol spot that is quite dark grey.

Shortwave (280–4,000 nm) surface solar flux measurements were carried out using Pyranometer (make Kipp & Zonen). The meteorological parameters like temperature, wind speed, wind direction and relative humidity were obtained using the AWS installed at GBPIHED, Himachal Unit, Mohal, Kullu (H.P.). The influence of aerosols in changing shortwave solar radiation were investigated taking into account long range transport using Hybrid Single Particle Lagrangian Integrated Trajectory (HYSPLIT) model (website: http://www.arl.noaa.gov/ready/hysplit4.html) along with Cloud-Aerosol Lidar and Infrared Pathfinder Satellite Observations (CALIPSO) (Winker et al. 2009).

In the present study, the most important input parameters for estimating the aerosol radiative forcing such as AOD, single scattering albedo (SSA) and asymmetry parameter (g) are retrieved from Optical Properties of Aerosol and Clouds (OPAC) database by adopting the external mixing approach (Hess et al. 1998). The OPAC model is run to estimate aerosol optical properties between 0.25 and 4.0 μm. As the measurements of aerosol chemical compositions were not available; we have used a hybrid approach to estimate aerosol optical properties. The zero-order approximation is performed by adopting polluted continental aerosol types (post-monsoon and winter months) and desert aerosol types (pre-monsoon and monsoon months) in the OPAC database. The earlier studies (Guleria et al. 2011a, b) have reported that transport of dust aerosols from the western desert contributes significantly to the existing concentration of coarse mode aerosols during pre-monsoon and monsoon seasons. Besides local sources, anthropogenic aerosols from the polluted continental region of India in post-monsoon and winter also contribute to the large concentration of fine mode aerosols. In view of possible sources of aerosols over Mohal, the choice of polluted continental and desert aerosol types in the OPAC database have been adopted. The OPAC model is run to reconstruct the AOD spectra taking AOD, α, and BC aerosol number concentration as the anchoring points.

The OPAC estimated optical properties of aerosols namely AOD, SSA and *g* are further used to calculate clear-sky radiative forcing in the shortwave region ranging from 0.25 to 4.0 µm by using radiative transfer model (RTM) based on the Discrete Ordinate Radiative Transfer (DISORT) module (Ricchiazzi et al. 1998). The DISORT method was first proposed by Chandrasekhar (1950) and later modified and improved by Liou (1973) and Stamnes et al. (1988). This radiative transfer code uses numerically stable algorithm to solve the equations of plane-parallel radiative transfer in vertically inhomogeneous atmosphere (Ricchiazzi et al. 1998). Following successful applications in modeling the radiative transfer, the DISORT method has become most popular among atmospheric and space research community (Ricchiazzi et al. 1998; Moorthy et al. 2005; Jin et al. 2006; Pant et al. 2006; Babu et al. 2007; Pathak et al. 2010; Singh et al. 2010). The RTM is run to compute plane-parallel radiative transfer in cloud-free days within the atmosphere-land system. The clear-sky shortwave aerosol radiative forcing calculations are performed separately with and without aerosols at 5° zenith interval and are used to determine 24 h averages.

3 Results and Discussion

3.1 AOD—Forenoon and Afternoon

The full day mean AOD values at ten wavelengths (380, 400, 450, 500, 600, 650, 750, 850, 935, 1,025 nm) for the clear-sky days for the last 5 years from 2006 to 2010 were obtained. Based on the study, it was found that AOD values were noticed maximum for the year 2010 and minimum for the year 2007 (Fig. 1a). On average, the AOD value at 500 nm was 0.22 in 2007 which increased up to 0.27 in 2010. This increase was 22 % between 2007 and 2010. The fine size aerosols as AOD within accumulation and fine mode (380–500 nm) are supposed to
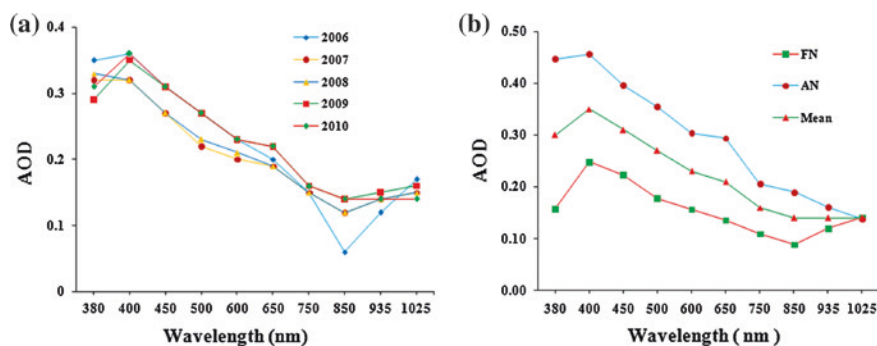

Fig. 1 Columnar aerosols: **a** AOD values (2006–2010), and **b** FN, AN, mean AOD for the year 2010

be produced due to anthropogenic interferences, which ranged from 0.28 to 0.31 AOD, an increase by 10.71 % at the rate of 3.57 % per annum. While the AOD values, on average, for coarse size particles (600–1,025 nm) were found in a range from 0.16 to 0.17, an increase by 6.25 % at the rate of 3.1 % per annum from 2007 to 2010. Primary reasons of increase from 2006 to 2010 are possibly the defor-estation, sprawling urban towns (or urbanization), industrialization (like cement plants, etc.), upcoming hydropower projects, forest fires, vehicular emissions, open waste burning, etc. It is found that the AOD values are higher at shorter wavelengths and lower at larger wavelengths indicating dominance of anthropo-genic aerosols over natural ones. As a day advances from forenoon to afternoon (FN to AN), temperature of the Earth's atmosphere also increases. As a result, the process of lifting air pollutants or aerosols above the ground due to convective process gets dispersed at higher levels (Kuniyal et al. 2009).

This convective process results in relatively higher concentration of aerosols during afternoon (Fig. 1b). In addition, it is observed that the long range transport of aerosols also increase the atmospheric turbidity level. The cool air mass flow laden with finer size air pollutants at lower height reaches at its peak during after-noon when local air gets warm up due to relatively stronger sunshine and outside cool air takes its place. The highest annual forenoon AOD during the clear sky days at 500 nm was 0.59 on 30 May 2006, while its lowest value was 0.33 on 24 November 2010. At the same time, the maximum afternoon AOD for the clear sky days at 500 nm was 0.76 on 19 March 2010 and lowest value was 0.48 on 22 April 2007 as well as on 31 January 2008. It is therefore observed that AOD values at forenoon are lower than those of observed values at afternoon.

3.2 Variations in Ångström Exponent (α) and Turbidity Coefficient (β)

Ångström parameters such as wavelength exponent (α) and turbidity coefficient (β) indicate size distribution of the scattering particles and total aerosol content respec-tively. In a majority of the cases, it is found that α and β were inversely proportion-ate to each other (Fig. 2a). The monthly mean value of α and β for the clear sky days recently in 2010 was also obtained. When α values remain very small or say of the order of air molecules, it may approach up to 4 while in case of very large size parti-cles, it may be as low as 0 (Holben et al. 2001; Pinker et al. 2001). Ångström expo-nent 'α' as the maximum was 1.54 in the month of August and minimum was 0.54 in the month of March indicating dominance of finer size aerosols in August over the other months of a year. While the maximum value of the 'β' was 0.31 in the month of July and the minimum was 0.07 in the month of August indicating the maximum visibility in the atmosphere in August due to very low turbidity.

One of the reasons for high visibility and low turbidity in the month of August in 2010 may be due to washout effects of rainfall when maximum sixteen rainy days during this month were recorded. Due to increase in α, the fine particle
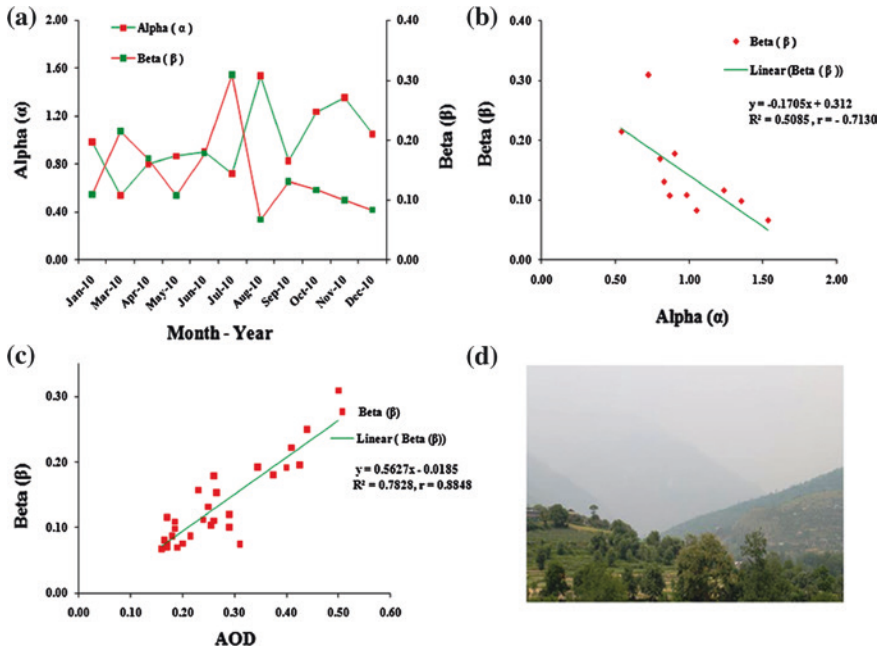
Fig. 2 Ångström parameters: **a** monthly mean values of α and β for the year 2010, **b** correlation coefficient between α and β, **c** correlation coefficient between AOD, β, and **d** a view of hazy atmosphere in the Kullu valley

concentrations increase (Dumka et al. 2008). The peculiar feature in case of fine particles is that these have maximum heat absorbing capacity that result in warming effect for longer duration in the atmosphere. However, increase in β indicates increase in the total particles leading to turbidity in the atmosphere that cause low visibility. While the correlation coefficient between α and β for the clear sky days of the year 2010 unfolds it to be $r = -0.713$ indicating strong negative correlation between these two Ångström parameters. In other words, when α increases, β decreases and vice versa (Fig. 2b).

The correlation coefficient between AOD at 500 nm and β for the clear sky days in 2010 estimated to be $r = 0.88$ indicating strong positive correlation between AOD and β (Fig. 2c). This means that when AOD value increases, β value also increases. In other words, when coarse size particles increase, there is also an increase in AOD values resulting in turbidity conditions in the atmosphere (Fig. 2d).

3.3 AOD and Black Carbon Aerosol

The diurnal variation in BC aerosol mass concentrations is influenced partly by the diurnal vertical increase in the atmospheric boundary layer (ABL) (Ganguly et al.

2006; Pathak et al. 2010) and partly by increasing human activities in the forms of vehicular emissions and biomass burning. The ABL is low during morning time, thereafter gradually rises with increasing sunshine hours up to its maximum level by noon. When sun sets, BC starts to decrease by the evening hours. In early morning hours, the sharp increase in the production of BC aerosol mass concentrations is mainly attributed to the dynamics of the local ABL. Besides, routine activities of the households and commuters in the form of biofuel or biomass/fuel wood burning might also be contributing to its existing level of concentration. After sunrise, the ABL starts to uplift which results in thermal strengthening that lifts up the BC aerosols and eventually breaks the nighttime inversion. This gradual formation of a surface based inversion opposes vertical mixing in the atmosphere causing aerosols to mix in the residual layer with those aerosols near the surface which lead to a sharp increase in the near-surface concentrations.

This effect in such a way caused is known as fumigation (Stull 1998; Fochesatto et al. 2001). Because of this effect, the primary peak generally is observed around 8.00 to 9.00 h Indian Standard Time (IST). As the day advances, the ABL is lifted at its highest level due to warming of the Earth's surface through solar energy and thereafter it gets weakened as the sun sets resulting in low BC production in the ambient air near the surface. This atmospheric process results in sharp decrease in the BC aerosol mass concentrations. During sunset hours, the burden of anthropogenic activities were realized in the form of vehicular influx, open waste burning, burning of crop residues, forest fire, and fuel wood burning to keep the house temperature warm. During winter, it again starts to increase from around 16.00 h IST and reaches at its peak by around 20.00 h IST. Moreover, the radiative cooling of the ground surface results in suppression of turbulent mixing and consequently increases the possibility of aerosol concentrations during early night.

The gradual increase in BC aerosol mass concentrations from around 16.00 h IST is considered to be due to alike anthropogenic activities and gradual formation of a surface based inversion opposing vertical mixing in the atmosphere (Ganguly et al. 2006; Nair et al. 2007). After reaching at its secondary maxima, the BC aerosol mass concentrations decreases gradually because of low anthropogenic activities during this period.

The hourly highest ever BC aerosol mass concentration was observed as 32,447 ng m^{-3} on December 28, 2009 at 8.00 h IST and 33,764 ng m^{-3} on January 12 at 7.00 h IST. The monthly mean values of BC aerosols at Mohal in 2010 are shown in Fig. 3. Its monthly mean concentration was noticed maximum with 6,617 ng m^{-3} in January, 2010 and minimum with 3,259 ng m^{-3} in June, 2010. In general, the BC aerosol mass concentration increases with an increase in human activities like vehicular emissions, biomass burning (fuel wood for cooking), forest fires, etc. The average of FN and AN AOD at 500 nm for a full day was compared with the average of BC aerosol mass concentration over a period of 2010 year for the clear sky days (see Fig. 3). The BC aerosols are primarily from the anthropogenic sources (Badrinath and Kharol 2008), while the AOD sources are from both the sources; natural and anthropogenic.

Fig. 3 Black carbon (BC)
aerosols concentrations at
Mohal-Kullu, 2010
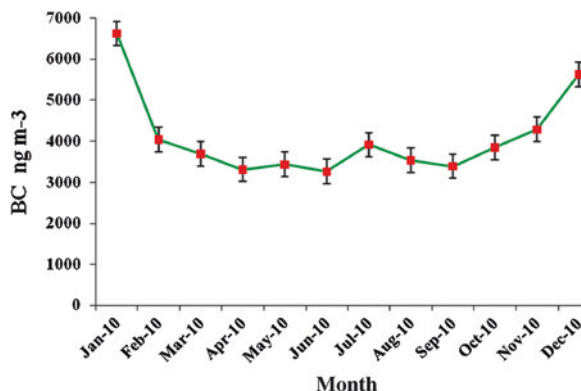
3.4 AOD and Meteorological Parameters

3.4.1 AOD and Temperature

The AOD values obtained at 500 nm were compared with the average values of
the temperature for a period of MWR operation during the clear sky conditions in
2010. It is found that the correlation coefficient between these two parameters was
weak positive ($r = 0.361$). However, increase in temperature leads to the convec-
tive process and aerosols are lifted up from the surface within ultra violet, visible,
and infrared spectrums.

3.4.2 AOD, Wind Speed and Wind Direction

The average values of AOD at 500 nm when was compared with the average val-
ues of wind speed for the clear sky days in 2010, it was found that the windblown
aerosols from the polluted regions reach to our study region. As a result, existing
concentration of aerosols also increase in our region. As the wind speed increases,
the AOD values also shoot up. The mean values of wind direction were from the
south-east and south direction to the present study region.

3.4.3 AOD, Back Trajectory and Satellite Data

For examining the possibility about the transport of trans-boundary pollutants
from the external sources to our study region, 7 day's back trajectories were
drawn using HYSPLIT model (Draxler and Rolph 2010). The back trajectories
were drawn at the three different heights 3,500 m, 5,500 m and 7,500 m above
the ground level (Fig. 4a). The trajectories drawn at 3,500 m AGL is influenced by
the activities generating pollutants within the valley, whereas trajectories at 5,500
and 7,500 m AGL are taken into account considering the surrounding hills of the
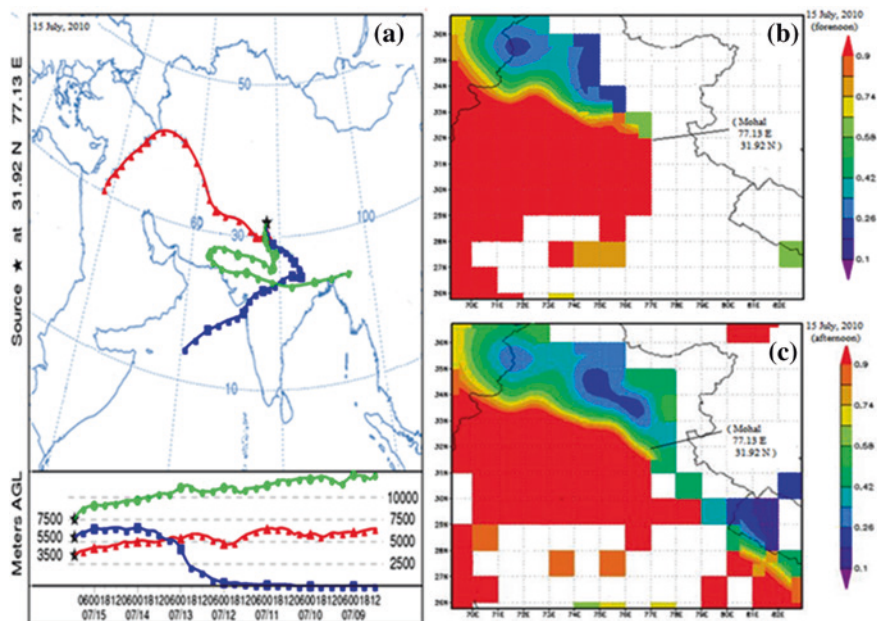
Fig. 4 Transported aerosols on July 15, 2010: **a** representing the back trajectory, **b** showing forenoon (Terra), and **c** afternoon (Aqua) AOD from MODIS satellite data

present experimental site located between 3,000 and 5,000 m (Sharma et al. 2009). The trajectories drawn at 5,500 and 7,500 m are influenced by the activities generating pollutants which are transported from the external sources outside the present study region—the Kullu valley.

The external sources of pollutants are sometimes from the other countries. The trajectories drawn at lower heights contribute to coarse size particles whereas at higher altitudes these contribute to the finer particles. A web based application known as GIOVANNI developed by Gooddard Earth Sciences Data and Information Science Centre (GESDISC) is used to establish relationship of our ground based measurements with the satellite based AOD at 550 nm. MODIS shows AOD for forenoon by using satellite Terra from the data product file MODO8_D3.051, while afternoon AOD was obtained using satellite Aqua from the data product file MYDO8_ D3.051. The products were MODIS Terra and Aqua Daily level-3 data (atmosphere daily global 1 × 1 degree) which were used in plotting the observation points over the land (website: http://www.disc.sci.gsfc. nasa.gov/Giovanni).

Based on the top four highest AOD values pinpointed during a recent past year 2010, it is observed that all these values ranged from 0.40 (June 19) to 0.50 (July 15) (Fig. 4b, c). When the back trajectory analysis in relation to MODIS data—Terra and Aqua for AOD is observed, it is found that the aerosol source regions during these 4 days were from the desert regions. The dust event of March 19,

2010, when AOD measured 0.44 through MWR, shows that all the three air masses at different altitudes were found to be a little bit influenced from the different directions.

However, when they reach covering half of the distance being covered during 7 days, they almost move together over the same places of the desert regions of the Middle East Countries and/or the Sahara Desert or over the places having more values of AOD ranging from 0.26 to 0.66 obtained through Terra and Aqua MODIS satellite data respectively. The other pollution episode, observed on April 6, 2010, shows 0.43 AOD from MWR while the regions through which the air masses move showed AOD in a range from 0.24 to 0.64 from MODIS—Terra and Aqua. In other words, it is made clear that these pollution episodes have been an outcome of external sources through air masses from the polluted regions. The event of pollution episode on June 19, 2010 also explains that the air mass at different three altitudes move from the three different directions. But the interesting part of these air masses before reaching to the present study region is that all these air masses move from the Sahara Desert. It is evident from these air masses that these passed through the highly polluted regions of Iran, Afghanistan and Pakistan.

3.5 AOD, Temperature Rise and Clear-Sky Shortwave Aerosol Radiative Forcing

During the observation period (2006–2010), the monthly 24-h average clear-sky shortwave aerosol radiative forcings (ARF) estimated at top of the atmosphere (TOA), surface (SFC), and atmosphere (ATM) were $+0.17 \pm 3.3$ W m^{-2}, -19.2 ± 2.1 W m^{-2} and $+19.4 \pm 3.7$ W m^{-2}, respectively. The clear-sky shortwave ARF varied from -6.4 to 6.1 W m^{-2}, -15 to -25.4 W m^{-2}, and $+15.1$ to $+29.0$ W m^{-2} at the TOA, SFC and ATM, respectively. The magnitude of ARF at the TOA can either be positive or negative which strongly depends on SSA (George 2001). The magnitude of TOA forcing is negative in pre-monsoon (-2.5 ± 2.0 W m^{-2}) and monsoon (-1.9 ± 1.3 W m^{-2}), whereas it is positive in post-monsoon ($+0.5 \pm 1.6$ W m^{-2}) and winter ($+4.0 \pm 1.7$ W m^{-2}). The seasonal maximum ARF at the surface occurred during pre-monsoon (-21.5 ± 2.1 W m^{-2}), while the minimum occurred during monsoon (-18.0 ± 1.3 W m^{-2}). During pre-monsoon, monsoon, post-monsoon and winter, the mean values of atmospheric forcing are estimated to be 19.0 ± 1.0 W m^{-2}, 16.0 ± 0.8 W m^{-2}, 19.9 ± 1.4 W m^{-2} and 23.0 ± 2.0 W m^{-2}, respectively. The highest value of atmospheric forcing in winter attributed to the absorptive properties of the aerosols. The aerosol forcing at the surface during pre-monsoon was about 1.2 times stronger than in winter. The considerable reduction in surface reaching solar radiation during pre-monsoon has increased the atmospheric forcing, which translates into a clear-sky atmospheric heating rate of 0.48 K day^{-1} in the 300 hPa thick aerosol layer. This strong response to aerosol forcing is attributed to enhanced loading of desert dust aerosols, which are mostly transported

from the western desert regions. The atmospheric heating rate during pre-monsoon, monsoon, post-monsoon, and winter varied between 0.43–0.53, 0.42–0.49, 0.52–0.62, and 0.52–0.81 K day^{-1}, respectively. For comparison, Ganguly and Jayaraman (2006), Babu et al. (2007), Sreekanth et al. (2007), and Pathak et al. (2010) have reported an average range of heating rate for different seasons over Dibrugarh, Ahmedabad, Visakhapatnam, and Trivandrum to be 0.35–1.0, 0.60–1.13, 0.09–1.23, and 0.62–1.51 K day^{-1} respectively.

In the present study, the minimum value of AOD at 500 nm (AOD = 0.10) is obtained on 8 March 2007 and is referred as a low aerosol loading day. During pre-monsoon, the average forcing at the surface and in the atmosphere is found to change by −13.0 and +9.8 W m^{-2}, respectively when compared with the estimated value of a low aerosol loading day. This implies that during pre-monsoon, the reduction in surface reaching solar radiation increased by 152 % when is compared with the low aerosol loading day. At the same time, the atmospheric heating rate noted to be 1.8 times higher than that of low aerosol loading day. During post-monsoon, the average forcing at the surface and in the atmosphere is found to change by −10.9 and +10.7 W m^{-2}, respectively when compared with the value of a low aerosol loading day. It means that during post-monsoon, the reduction in surface reaching solar radiation increased by 128 % when it is compared with low aerosol loading day and the atmospheric heating rate touched 2.2 times higher when is compared with low aerosol loading day.

Largest annual-mean surface aerosol forcing is estimated to occur in 2006 and 2010 (Table 1). In contrast, the negative TOA aerosol forcing is estimated for year 2006 and 2010. The atmospheric forcing increases if aerosol forcing at the TOA approaches towards positive, while there is a large negative forcing at the surface level. This cause-effect relationship is due to absorption by absorbing aerosols (Pathak et al. 2010). It means that during 2007–2009, Mohal has been influenced due to a large concentration of absorbing aerosols as compared to their concentrations in 2006 and 2010.

During 2006–2010, the maximum and minimum values of AOD at 500 nm are obtained as 0.50 and 0.10 on 4 June 2009 and 8 March 2007, respectively. About 57 % decrease in the Ångström exponent and 500 % increase in the turbidity coefficient is observed on 4 June 2009 as compared to 8 March 2007, suggesting a large loading of coarse-mode size aerosols in the atmosphere. The possible

Table 1 Annual-mean clear sky aerosol radiative forcing: at the Earth's surface, TOA and in the atmosphere over Mohal

| Year | Aerosol radiative forcing (W m^{-2}) | | | |
	TOA	Surface	Atmosphere	Heating rate (K day^{-1})
2006	−0.9	−19.5	18.5	0.52
2007	0.6	−18.5	19.1	0.54
2008	1.2	−18.9	20.1	0.56
2009	0.5	−19.1	19.6	0.55
2010	−0.6	−20.2	19.6	0.55

Fig. 5 Back trajectories ending at 06 UTC over Mohal drawn on highest AOD day at 500 nm, i.e., 4 June 2009, and CALIPSO derived vertical feature mask image (version: 3.01) showing large aerosol loading around 28.5°N, 50.0°E on 2 June 2009. The star denotes the location of Mohal
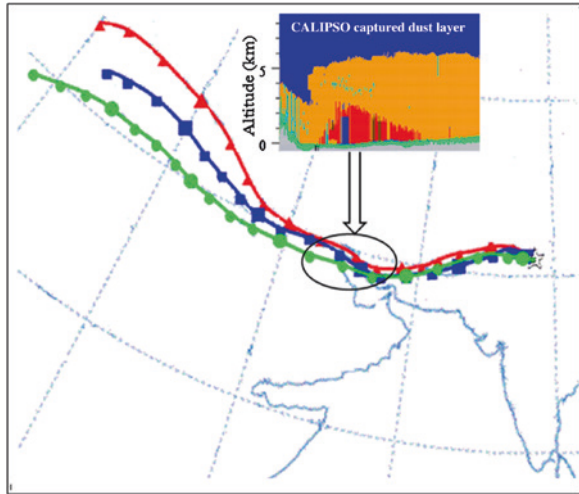
sources are investigated using the collective approach of CALIPSO and HYSPLIT model. The CALIPSO is a part of the A-Train constellation of satellites and has been making global measurement of aerosols and clouds since 13 June 2006 (Winker et al. 2009). The depolarization technique of the Cloud-Aerosol Lidar with Orthogonal Polarization (CALIOP) on board of CALIPSO satellite measurements is used to distinguish different variety of aerosols. After plotting back trajectories at different altitudinal heights, it was concluded that these air parcels originated in the Sahara Desert (Fig. 5). It was on 2 June 2009 when these air parcels passed through 28.5°N latitude, and 50.0°E longitude. At the same time, the CALIPSO pass was available which captured vertically an extended aerosol layer with a thickness of about 5 km (Fig. 5).

Moreover, the extinction-derived higher depolarization ratio (~0.4) profile derived from CALIOP suggested larger concentrations of dust particles. From the combined approach, it is known that the air-masses capture the dust while passing from around 28.5°N and 50.0°E and has increased the possibility to accumulate coarse-mode size particles over Mohal region. Figure 6 shows the influence of AOD on aerosol forcing estimated on 8 March 2007 and 4 June 2009. It can be seen from Fig. 6 that the enhanced loading of aerosols has a large impact with considerable reduction in surface reaching solar radiation. On 4 June 2009, the surface aerosol forcing is found to change by -14.7 W m^{-2} when is compared with 8 March 2007. Due to this large reduction in surface reaching solar radiation, the atmospheric heating touched 2.0 times higher on 4 June 2009 as compared to the value of 8 March 2007.

The notable reduction in surface reaching solar radiation estimated during a period of half decade (2006–2010) showed increasing atmospheric forcing, which translates into clear-sky atmospheric heating rate of 0.54 K day^{-1} in a 300 hPa thick aerosol layer with a month-to-month variations from 0.42 to 0.81 K day^{-1}. Such reduction in surface reaching solar radiation and increase in heating rate

Fig. 6 Aerosol radiative
forcing estimates on 8 March
2007 (a low aerosol loading
day) and 4 June 2009 (a high
aerosol loading day)
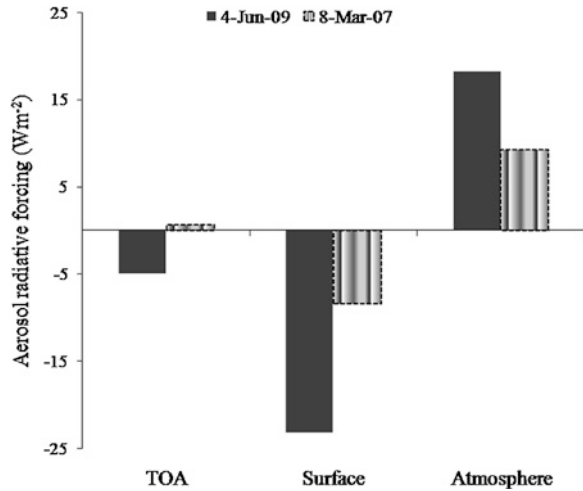
is responsible to cause changes in atmospheric thermal structure, synoptic and
regional circulation systems, suppression of rainfall and less efficient removal
of pollutants (Ramanathan and Feng 2009). The present study therefore reports
the atmospheric forcing and associated heating rate, which directly supports the
hypothesis of "Elevated Heat Pump", suggesting that absorbing aerosols over
the northwestern Indian Himalaya may cause enhanced heating in the middle
and upper troposphere, and may also lead to an early strengthening of the Indian
monsoon rainfall (Lau et al. 2006; Lau and Kim 2006). This study suggests that
while assessing the aerosol deposition (Ming et al. 2008; Qian et al. 2011) and
aerosol-induced warming effects (Lau et al. 2010; Qian et al. 2011) on the glacier
melting in the Himalayas, the seasonal variations in aerosol radiative forcing and
solar heating rate over Mohal will be helpful in future for the radiative and climate
impact assessments.

4 Conclusions

Aerosols have direct impact not only on the atmospheric visibility, air quality,
formation of dew, mist and fog, etc. but also on the human health, plant life and
more importantly on the climate. The study of aerosols in the Himalayan eco-
system is important because it will have long-term effects on temperature rise,
shifting of vegetation and crops, glacier melting and human health in a wider
altitudinal range from low to high. AOD values at shorter wavelengths are higher
than at larger wavelengths indicating high anthropogenic pressure in the present
study region which is increasing continuously. Afternoon AOD values are higher
than forenoon AOD values being favoured by the strong convective activity dur-
ing afternoon in presence of adequate solar flux. The monthly mean low Ångström

exponent values noticed during pre-monsoon season indicate dominance of coarse size particles, while higher Ångström exponent values during post-monsoon season show dominance of fine size particles in our atmosphere. The seasonal aerosol forcing at the surface is estimated maximum during pre-monsoon, while the minimum occurred during monsoon. The surface aerosol forcing during pre-monsoon is found to be about 1.2 times stronger than winter. This study shows that during pre-monsoon, the reduction in the solar radiation reaching the surface increased by 152 % when is compared with the estimated value of a low aerosol loading day. Largest annual-mean surface aerosol forcing is estimated during 2010, while the minimum occurred during 2007. The present study estimates reduction in solar radiation arriving at the surface together with the atmospheric warming from 0.42 to 0.81 K day^{-1} with a mean value 0.54 K day^{-1} at 300 hPa thick aerosol layer.

References

Ångström A (1961) Techniques of determining the turbidity of the atmosphere. Tellus 13:214–223

Babu SS, Moorthy KK, Satheesh SK (2007) Temporal heterogeneity in aerosol characteristics and the resulting radiative impacts at a tropical coastal station. Part 2: Direct short wave radiative forcing. Ann Geophys 25:2309–2320

Badrinath KVS, Kharol SK (2008) Studies on aerosols properties during ICARB-2006 campaign period at Hyderabad, India using ground-based measurements and satellite data. J Earth Syst Sci 117(S1):413–420

Beegum SN, Moorthy KK, Nair VS, Babu SS, Satheesh SK (2008) Characteristics of spectral aerosol optical depths over India during ICARB. J Earth Syst Sci 117:303–313

Bhuyan PK, Gogoi MM, Moorthy KK (2005) Spectral and temporal characteristics of aerosol optical depth over a wet tropical location in North East India. Adv Space Res 35:1423–1429

Chandrasekhar S (1950) Radiative Transfer. New York: Dover. ISBN 0-486-60590-6

Charlson RJ, Schwartz SE, Hales JM, Cess RD, Coakley JA, Hansen JE, Hofmann DJ (1992) Climate forcing by anthropogenic aerosols. Science 255:423–430

Draxler RR, Rolph GD (2010) Hybrid single-particle Lagrangian integrated trajectory model. Access via NOAA ARL READY website NOAA Air Resources Laboratory, Silver Spring, MD. http://ready.arl.noaa.gov/HYSPLIT.php

Dumka UC, Moorthy KK, Pant P, Hedge P, Sagar R, Pandey K (2008) Physical and optical characteristics of atmospheric aerosols during ICARB at Manora Peak, Nainital: a sparsely inhabited, high-altitude location in the Himalayas. J Earth Syst Sci 117(S1):399–405

Fochesatto GJ, Drobinski P, Flamant C, Guedalia D, Sarrat C, Flamant PH, Pelon J (2001) Evidence of dynamical coupling between the residual layer and the developing convective boundary layer. Boundary-Layer Meteorol 99:451–464

Fu Q, Liou KN (1992) On the correlated *k*-distribution method for radiative transfer in non-homogenous atmospheres. J Atmos Sci 49:2139–2156

Fu Q, Liou KN (1993) Parameterization of the radiative properties of cirrus clouds. J Atmos Sci 50:2008–2025

Ganguly D, Jayaraman A (2006) Physical and optical properties of aerosols over an urban location in western India: implications for shortwave radiative forcing. J Geophys Res, 111, D24–D207, doi:10.1029/ 2006JD007393

Ganguly D, Jayaraman A, Gadhavi H (2006) Physical and optical properties of aerosols over an urban location in western India: seasonal variabilities. J Geophys Res 111:D24206. doi:10.10 29/2006JD007392

George JP (2001) Shortwave radiative forcing by mineral dust aerosols over Arabian Sea: a model study. Curr Sci 80:97–99

Gogoi MM, Bhuyan PK, Moorthy KK (2008) Estimation of the effect of long-range transport on seasonal variation of aerosols over northeastern India. Ann Geophys 26:1365–1377

Gogoi MM, Bhuyan PK, Moorthy KK (2009) An investigation of aerosol size distribution properties at Dibrugarh: North-Eastern India. Terrestrial Atmos Oceanic Sci 20:521–533

Guleria RP, Kuniyal JC, Rawat PS, Thakur HK, Sharma M, Sharma NL, Singh M, Chand K, Sharma P, Thakur AK, Dhyani PP, Bhuyan PK (2011a) Aerosols optical properties in dynamic atmosphere in the north western part of the Indian Himalaya: a comparative study from ground and satellite based observations. Atmos Res 101:726–738

Guleria RP, Kuniyal JC, Rawat PS, Sharma NL, Thakur HK, Dhyani PP, Singh M (2011b) The assessment of aerosol optical properties over Mohal in the northwestern Indian Himalaya using satellite and ground based measurements and an influence of aerosol transport on aerosol radiative forcing. Meteorol Atmos Phys 113 doi:10.1007/s00703-011-0149-5

Hansen ADA (2005) The Aethalometer Magee Scientific Company Berkeley, California, pp 1–207

Hansen ADA, Rosen H, Novakov T (1984) The aethalometer: an instrument for the real-time measurements of optical absorption by aerosol particles. Sci Total Environ 36:191–196

Hess M, Koepke P, Schult I (1998) Optical properties of aerosols and clouds: the software package OPAC. Bull Am Meteorol Soc 79:831–844

Holben BN, Tanre D, Smirnov A, Eck TF (2001) An emerging ground-based aerosol climatology: aerosol optical depth from AERONET. J Geophys Res 106:12067–12097

IPCC (2007) Climate change: the physical science basis. Cambridge University Press, Cambridge

Iqbal M (1983) An introduction to solar radiation. Academic Press, New York

Jin Z, Charlock TP, Rutledge K, Stamnes K, Wang Y (2006) Analytical solution of radiative transfer in the coupled atmosphere-ocean system with a rough surface. Appl Opt 45:7443–7455

Kuniyal JC, Rao PSP, Momin GA, Safai PD, Tiwari S, Ali K (2007) Trace gases behaviour in sensitive areas of the northwestern Himalaya-A case study of Kullu-Manali tourist complex, India. Indian J Radio Space Phys 36:197–203

Kuniyal JC, Thakur A, Thakur HK, Sharma S, Pant P, Rawat PS, Moorthy KK (2009) Aerosols optical depths at Mohal-Kullu in the northwestern Indian Himalayan high altitude station during ICARB. J Earth Syst Sci 118(1):41–48

Lau KM, Kim KM (2006) Observational relationships between aerosol and Asian monsoon rainfall, and circulation. Geophys Res Lett 33:L21810. doi:10.1029/2006GL027546

Lau KM, Kim MK, Kim KM (2006) Asian summer monsoon anomalies induced by aerosol direct forcing: the role of the Tibetan Plateau. Clim Dyn 26:855–864. doi:10.1007/s00382-006-0114-z

Lau KM, Kim MK, Kim KM, Lee WS (2010) Enhanced surface warming and accelerated 5 snow melt in the Himalayas and Tibetan Plateau induced by absorbing aerosols. Environ Res Lett 5:025204. doi:10.1088/1748-9326/5/2/025204

Liou KN (1973) Numerical experiment on Chandrasekhar's discrete ordinate—method for radiative transfer: applications to cloudy and haze atmosphere. J Atmos Sci 30:1303–1326

Liu SC, McKeen SA, Madronich S (1991) Effect of anthropogenic aerosols on biologically active ultraviolet radiation. Geophys Res Lett 8:2265–2268

Liu Z, Liu D, Huang J, Vaughan M, Uno I, Sugimoto N, Kittaka C, Trepte C, Wang Z, Hostetler C, Winker D (2008) Airborne dust distributions over the Tibetan Plateau and surrounding areas derived from the first year of CALIPSO lidar observations. Atmos Chem Phys 8:5045–5060

Ming J, Cachier H, Xiao C, Qin D, Kang S, Hou S, Xu J (2008) Black carbon record based on a shallow Himalayan ice core and its climatic implications. Atmos Chem Phys 8:1343–1352. doi:10.5194/acp-8-1343-2008

Moorthy KK, Nair PR, Murthy BVK (1991) Size distribution of coastal aerosols: effects of local sources and sinks. J Appl Meteor 30:844–852

Moorthy KK, Nair PR, Murthy BVK, Satheesh SK (1996) Time evolution of the optical effects and aerosol characteristics of Mt. Pinatubo origin from ground-based observations. J Atmos Terr Phys 58:1101–1116

Moorthy KK, Satheesh SK, Murthy BVK (1998) Characteristics of spectral optical depths and size distributions of aerosols over tropical oceanic regions. J Atmos Terr Phys 60:981–992

Moorthy KK, Niranjan K, Narasimhamurthy B, Agashe VV, Murthy BVK (1999) Aerosol climatology over India, ISRO-GBP MWR network and data base. Scientific report, SR-03-99. Indian Space Research Organisation, Bangalore

Moorthy KK, Babu SS, Satheesh SK (2005) Aerosol characteristics and radiative impacts over the Arabian Sea during intermonsoon season: results from ARMEX field campaign. J Atmos Sci 62:192–206

Nair VS, Moorthy KK, Alappattu DP, Kunhikrishnan PK, George S, Nair PR, Babu SS (2007) Wintertime aerosol characteristics over the Indo-Gangetic Plain (IGP): impacts of local boundary layer processes and long-range transport. J Geophys Res 112:D13205. doi:10.1029/2006JD008099

Pant P, Hegde P, Dumka UC, Sagar R, Satheesh SK, Moorthy KK, Saha AM, Srivastava MK (2006) Aerosol characteristics at a high altitude location in Central Himalayas: optical properties and radiative forcing. J Geophys Res 111:D17206. doi:10.1029/2005JD006768

Pathak B, Kalita G, Bhuyan K, Bhuyan PK, Moorthy KK (2010) Aerosol temporal characteristics and its impact on shortwave radiative forcing at a location in the northeast of India. J Geophys Res 115:D19204. doi:10.1029/2009JD013462

Pinker RT, Pandithurai G, Holben BN, Dubovik O, Aro TO (2001) A dust out break episode in sub-sahel West Africa. J Geophys Res 106(22):923–930

Qian Y, Flanner MG, Leung LR, Wang W (2011) Sensitivity studies on the impacts of Tibetan Plateau snowpack pollution on the Asian hydrological cycle and monsoon climate. Atmos Chem Phys 11:1929–1948. doi:10.5194/acp-11-1929-2011

Raju MP, Safai PD, Rao PSP, Devara PCS, Budhavant KB (2011) Seasonal characteristics of black carbon aerosols over a high altitude station in southwest India. Atmos Res 100:103–110

Ramanathan V, Feng Y (2009) Air pollution, greenhouse gases and climate change: global and regional perspectives. Atmos Environ 43:37–50

Ricchiazzi P, Yang SR, Gautier C, Sowle D (1998) SBDART: a research and teaching software tool for plane-parallel radiative transfer in the Earth's atmosphere. Bull Am Meteorol Soc 79(10):2101–2114

Satheesh SK, Moorthy KK, Das I (2001) Aerosol spectral optical depths over the Bay of Bengal, Arabian Sea and Indian Ocean. Curr Sci 81(12):1617–1625

Sharma NL, Kuniyal JC, Singh M, Negi AK, Singh K, Sharma P (2009) Number concentration characteristics of ultrafine aerosols (atmospheric nanoparticles/aitken nuclei) during 2008 over western Himalayan region, Kullu-Manali, India. Indian J Radio Space Phys 38:326–337

Shaw GE, Reagan JA, Herman BM (1973) Investigations of atmospheric extinction using direct solar radiation measurement made with a Multiple Wavelength Radiometer. J Appl Meteor 12:374–380

Singh M, Singh D, Pant P (2008) Aerosols characteristics at Patiala during ICARB-2006. J Earth Syst Sci 117(S1):407–411

Singh S, Soni K, Bano T, Tanwar RS, Nath S, Arya BC (2010) Clear-sky direct aerosol radiative forcing variations over mega-city Delhi. Ann Geophys 28:1157–1166

Sreekanth V, Niranjan K, Madhavan BL (2007) Radiative forcing of black carbon over eastern India. Geophys Res Lett 34:L17818. doi:10.1029/2007GL030377

Stamnes K, Tay SC, Wiscombe WJ, Jayweera K (1988) Numerically stable algorithm for discrete-ordinate-method radiative transfer in multiple scattering and emitted media. Appl Opt 27:2502–2509

Stull RB (1988) An introduction to boundary layer meteorology. Kluwer Academic Publishers, Dordrecht 670

Winker DM, Vaughan MA, Omar A, Hu Y, Powell KA, Liu Z, Hunt WH, Young SA (2009) Overview of the CALIPSO mission and CALIOP data processing algorithms. J Atmos Oceanic Technol 26:2310–2323